Publications of the Astronomical Society of the Pacific
106: 1258–1270, 1994 December

Deep *UBVRI* Photometric Calibration of High-Latitude Fields: SA 57 (1307+30) and Hercules (1720+50)

S. R. MAJEWSKI[1,2]

The Observatories of the Carnegie Institution of Washington, 813 Santa Barbara Street, Pasadena, California 91101
and Yerkes Observatory, P. O. Box 258, Williams Bay, Wisconsin 53191
Electronic mail: srm@ociw.edu

R. G. KRON[1]

Yerkes Observatory, P. O. Box 258, Williams Bay, Wisconsin 53191
Electronic mail: rich@oddjob.uchicago.edu

D. C. KOO[1] AND M. A. BERSHADY[2]

University of California Observatories, Lick Observatory and Board of Studies in Astronomy and Astrophysics,
University of California, Santa Cruz, California 95064
Electronic mail: koo@lick.ucsc.edu, mab@astro.psu.edu

Received 1994 August 23; accepted 1994 September 23

ABSTRACT. We present CCD photometric calibration sequences in the magnitude range $V=17-22$ for two fields at high Galactic latitude: SA 57 (at the North Galactic Pole) and Hercules ($l=77$, $b=35$). Photometry to a precision of about 0.02 mag at $V=20$ and, in general, better than 0.10 mag at $V=22$ was obtained in the Johnson *UBV* as well as the Kron–Cousins *R* and *I* bands. These data are suitable for setting magnitude zero-points in catalogues of faint stars, galaxies, and QSOs, and we apply them to our own photographic catalogs in these two fields. We also note a significant deviation in the $(V-R,R-I)$ color–color diagram for the locus of faint ($V>20$) M dwarfs compared to the locus provided by much brighter M dwarfs. This deviation may indicate differences in spectral properties between Population I and older populations of late dwarfs; however we do not discount the possibility that this locus for the faint stars, which appears as a saturation in $V-R$ color with increasing $R-I$ color, is the result of systematic photometric error.

1. INTRODUCTION

Since 1974, we have amassed a large collection of *U*-, *J*-, *F*-, and *N*-band Mayall 4-m plates in several selected areas for use in a variety of faint survey projects. These have included surveys of faint field galaxies (Kron 1980; Hamilton 1985; Koo 1985,1986; Bershady et al. 1994; Smetanka 1994), radio galaxies (Windhorst et al. 1984), and stars (Chiu 1980; Majewski 1992),[3] QSOs (Koo et al. 1986; Koo and Kron 1988; Trevese et al. 1994), and distant H II galaxies (Koo et al. 1994). The four regions in which we have concentrated our research programs were originally selected on the basis of high Galactic latitude, low extinction based on the Shane-Wirtanen (1967) galaxy counts, and a central asterism for easy identification. The first two fields so selected, SA 57 and SA 68, had established photoelectric standard sequences in *UBV*, but in general these sequences merely anchored the bright end of our work, near the point where stellar images on the photographic plates begin to saturate. Our other two fields, Hercules and SA 28, were selected to be approximately evenly spaced in right ascension from the first two (while remaining at high Galactic latitude), but are presently without published photometric sequences. Because work on the various surveys is continuing, deep, accurate photometric calibration of the fields is desired.

As part of a faint galaxy imaging project, a number of CCD frames were obtained in sections of the SA 57 and Hercules fields, with reference images taken of a standard star field in the globular cluster M92. As the observing run was photometric throughout, these data provide an opportunity to develop faint photometric sequences through standard stellar photometric analysis, accounting for airmass and color terms. We present here faint CCD photometric stellar sequences in our photographic SA 57 and Hercules fields that are adequate for setting magnitude zero-points in the Johnson *UBV* and Kron–Cousins *RI* bands.

Faint photometric sequences are needed for use with large aperture telescopes where bright standard sequences become impractical (requiring special arrangements to diminish or redistribute their flux, e.g., through defocusing, stopping down the telescope aperture, using neutral density filters, or the use of short integrations subject to shuttering errors and, for smaller apertures, to scintillation variations). Presently, very few faint sequences exist in the literature, and the most commonly used sequences are in globular cluster fields (for example, the KPNO Consortium fields of Christian et al. 1985), which means that very few main-sequence stars are included, and, in addition, there is a limited range in colors and metallicities. At least one long-term program is in progress by A.U. Landolt (cf. Landolt 1992) to establish very faint sequences of common field stars, but the results of that program have not yet been published. While the present program is by no means as ambitious, the sequences are provided here as part of this same general goal.

The SA 57 field, which contains a faint red–blue star pair

[1]Visiting Astronomer, Kitt Peak National Observatory, operated by the Association of Universities for Research in Astronomy, Inc., under contract with the National Science Foundation.
[2]Hubble Fellow.
[3]These nine references are all Ph.D. dissertations.

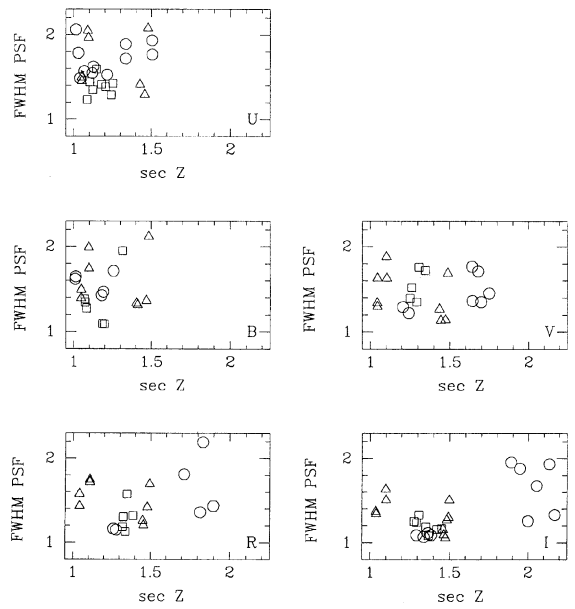

FIG. 1—The distribution of airmass (sec Z) and seeing for the M92 (triangles), SA 57 (circles) and Hercules (squares) CCD frames. The ordinate shows the FWHM of the PSF in arcseconds.

with a separation of 18.5 arcsec, is also listed as a faint Faint Object Camera (FOC) photometric sequence field by Bohlin et al. 1990). This particular field was selected not only because it contained a pair of stellar objects that met requirements for the calibration standards for the *HST*-FOC (color, magnitude, and separation), but also because the known proper motions guaranteed them to be stars. The Hercules field was chosen to include the radio galaxy 53W077 (see Windhorst et al. 1984) and also because this field has a relatively lower stellar density of bright stars for its Galactic latitude ($b=35°$) than other areas in our photographic catalog, a motivation driven by our faint galaxy imaging program. In another paper, we will describe the separate calibration of our fields in SA 28 (0842+45; also referred to as "Lynx") and SA 68 (0015+16).

2. OBSERVATIONS

Observations were obtained with the 320×512 RCA#1 CCD camera (with gain 10.5 electrons/ADU, readout noise 75 electrons rms, 30 μm pixels or 0.59 arcsec each) at the prime focus of the Mayall 4-m telescope during the nights of 1986 June 9–11 as part of a deep CCD imaging project. The seeing ranged from 1–2 arcsec full width at half maximum (FWHM), as shown in Fig. 1. All indications are that these nights were photometric, except for some thin cirrus on the beginning of the first night. This is shown, for instance, in the first three columns of Table 2 (see Sec. 3) where we obtain the same nightly zero-points within the derived errors in the instrumental photometric transformation functions. In addition, we find only very small net magnitude offsets in the reductions of standard star frames taken over the course of the run. Our data were taken with the (then) standard 4-m "Mould" filter set, and we utilized a glass U-band filter (before the liquid $CuSO_4$+UG-2 combination became the preferred standard). Some deterioration of the Mould filter set was noted at about the time of the observations (cf. Jacoby and Kinman 1986).

To partially overcome pixel-to-pixel quantum efficiency variations, and because of the significant fringing (especially in the red) due to the interference of night-sky emission lines, which can also vary throughout the night, we took advantage of the scanning capabilities of the KPNO 4-m dewar assembly. The majority of our observations were taken in the "short-scan" mode. As we were the first general users of the system, some experimentation with the number of scan rows was necessary, with the result that images of our target fields were taken at a variety of scan values: 0, 16, 32, and 64 rows. We found no systematic photometric differences as a function of the number of scan lines. The short-scanning significantly reduced, but did not entirely eliminate in the redder bands, fringe patterns in the final images; residual fringe amplitudes were sufficiently small (less than 1%–2%) to be ignored for the precision of the photometry we desired. Exposures of our standard star-calibration sequence in the M92 field were necessarily short, 15–30 s, so that scanning was turned off for expediency. In addition to the scanning, random dithers on the order of tens of arcseconds were applied between exposures of the same field in the same passband. Because of the large readout noise (75 electrons rms) in the RCA detector, and the low U-band surface brightness of the night sky, relatively long exposures of SA 57 and Hercules were used in order to reach the sky-noise-limited regime. Five to 11 exposures were taken of M92, the Hercules field, and the SA 57 field in each band. For the latter two fields, the integration times for individual exposures were typically around 30, 3, 3, 3, and 4 min for the U, B, V, R, and I bands, respectively.

The CCD frames were reduced using the IRAF[4] package CCDRED and made use of medians of several dozen bias frames and dome flats (scaled to a common mean value) within each filter. The bias frames showed a nightly variation and a separate bias was used for each night. Dome flats were obtained in both scanning and nonscanning mode. No systematic differences were found when the scanned dome flats were compared to scanned images created synthetically by repeatedly shifting and adding the unscanned dome flats. An advantage however is gained through the use of dome flats scanned synthetically via software shifting and adding since in this case the pixels in the resultant image have been smoothed over N pixels after readout by the electronics, which results in a decrease of the contribution of the readout noise by $N^{1/2}$ per pixel. In general, we found the dome flats adequate to flatten our images to better than 1%. However, because the quartz projection lamp used to illuminate the Kitt Peak 4-m "Great White Spot" is much redder than the night sky, the dome-flattened U images suffered from large-scale nonuniformities at the 1% level. High signal-to-noise

[4]IRAF is a product of the National Optical Astronomy Observatories which is operated by the Association of Universities for Research in Astronomy, Inc., under contract with the National Science Foundation.

TABLE 1
Adopted M92 Calibration Sequence Magnitudes

ID	V	$e(V)$	$U-B$	$e(U-B)$	$B-V$	$e(B-V)$	$V-R$	$e(V-R)$	$R-I$	$e(R-I)$	Other ID
01	13.0973	0.0122	+0.020	0.008	+0.6051	0.0163	+0.257	0.060	+0.421	0.119	
02	14.5983	0.0142	+0.109	0.025	+0.7931	0.0212	+0.485	0.009	+0.461	0.033	
03	14.7135	0.0062	+0.093	0.017	+0.7838	0.0121	+0.485	0.017	+0.454	0.018	
04	14.6325	0.0043	+0.111	0.018	+0.7759	0.0066	+0.486	0.014	+0.464	0.035	IX-10
05	16.0721	0.0026	−0.111	0.013	+0.5227	0.0069	+0.313	0.008	+0.277	0.005	IX-9
06	16.3500	0.0042	−0.442	0.012	−0.1090	0.0058	−0.038	0.010	−0.085	0.005	IX-8
07	16.4553	0.0037	−0.478	0.004	−0.1133	0.0058	−0.041	0.010	−0.086	0.020	IX-26
08	15.9440	0.0027	−0.079	0.009	+0.5540	0.0043	+0.351	0.015	+0.302	0.019	IX-25
09	17.0079	0.0034	+1.124	0.044	+1.1431	0.0069	+0.722	0.008	+0.589	0.029	IX-100
10	14.0538	0.0025	+0.325	0.029	+0.7949	0.0036	+0.516	0.014	+0.417	0.014	A
11	15.1649	0.0010	+0.844	0.030	+1.0090	0.0049	+0.630	0.020	+0.522	0.019	
12	15.9930	0.0049	−0.026	0.014	+0.6772	0.0079	+0.433	0.013	+0.411	0.013	
15	17.1723	0.0093	−0.129	0.004	+0.6221	0.0292	+0.396	0.019	+0.361	0.015	
16	15.2813	0.0047	+0.061	0.020	+0.0811	0.0125	+0.058	0.017	+0.049	0.005	
17	14.4921	0.0029	−0.015	0.044	+0.5663	0.0096	+0.403	0.016	+0.362	0.030	
18	17.9851	0.0066	−0.247	0.061	+0.4860	0.0161	+0.320	0.005	+0.320	0.007	
19	18.2320	0.0065	−0.317	0.214	+0.4144	0.0104	+0.286	0.018	+0.273	0.008	
21	17.9431	0.0037	−0.188	0.014	+0.4900	0.0058	+0.340	0.009	+0.296	0.014	
22	17.5765	0.0053	−0.254	0.039	+0.5374	0.0080	+0.357	0.017	+0.323	0.020	C
23	16.8142	0.0046	−0.132	0.017	+0.6282	0.0064	+0.403	0.006	+0.368	0.043	B

exposures of twilight sky were used to make the necessary "skyflat" correction in the U band.

3. PHOTOMETRIC REDUCTIONS

3.1 Aperture Photometry

Photometric reductions were done using the IRAF aperture photometry package APPHOT. For each frame, the stars selected to define the photometric sequence were fit to circular Gaussians to determine their centroids and point-spread functions (PSFs). From an average of these stars, the FWHM of the PSF was determined for each frame. An aperture of radius 3.0×FWHM of the PSF was used to measure the flux from each sequence star. The sky flux was estimated by the mode of the distribution of pixels in an annulus about each object of radii 5 to 15 times the FWHM, after a 3 sigma rejection of pixels contaminated by neighboring objects, chip defects, or cosmic rays. Photometry was also done on several bright, compact galaxies in each field to provide additional objects for setting magnitude zero-points. Figure 1 shows the distribution of FWHM for the frames taken in the course of the observing run.

Note that no corrections were made to the frames to remove bad pixels or cosmic rays. All images near bad columns, pixels, and cosmic rays were noted and removed from the photometric solutions if their photometric apertures included the defect. This was more of a problem than usual, since in scanning mode all bad pixels in the CCD array get smeared across N rows. The result with RCA#1 was a "picket fence" effect near some problem areas that obliterated otherwise useful photometric measures in these areas. In hindsight, the aperture size used here was larger than optimal: while large enough to include nearly all stellar flux and reduce the effects of centroid errors, more measures were discarded due to contamination by cosmic rays and chip defects than would have been necessary had smaller apertures been used. In addition, there was greater incidence of contamination of larger apertures by nearby objects, especially in images having large PSFs.

3.2 Transformation Equations

Calibration was made via comparison to short exposures of the Kitt Peak Video Camera/CCD Standards Consortium field of the globular cluster M92 (Christian et al. 1985, Heasley and Christian 1986). Stetson and Harris (1988) have produced a high-quality $(V,B-V)$ color–magnitude diagram for this cluster and we have adopted their ultimate set of adopted B and V magnitudes, which represent an average of their data and previous work, as given in their Table IV(c).[5] Note that the Stetson and Harris M92 data were taken just after the nights as the present data, on the same mountain. The adopted U, R, and I magnitudes for the M92 sequence were obtained by combining the Stetson and Harris B or V magnitude and the appropriate colors from an unpublished calibration of $(U-B)$, $(V-R)$, and $(R-I)$ by Lindsey Davis (1986, private communication).[6] The adopted M92 magnitudes are summarized in Table 1.

Instrumental magnitudes (u,b,v,r,i) for these M92 stars were fit to equations of the form

$$u-U=k_{1,j}+k_2X+k_3(U-B)+k_4X(U-B)+k_5(U-B)^2, \quad (1a)$$

[5]For stars 1, 2, and 15, which are not given in Table IV(c) of Stetson and Harris (1988), we applied the mean correction by Stetson and Harris to the Davis values.

[6]Because Davis quotes errors in only V magnitude and in colors, the relative errors in the adopted M92 U, R, and I magnitudes were approximated as

$$\sigma^2(U)=\sigma^2(U-B)+\sigma^2(B),$$
$$\sigma^2(R)=\sigma^2(V-R)+\sigma^2(V),$$
$$\sigma^2(I)=\sigma^2(R-I)+\sigma^2(V-R)+\sigma^2(V),$$

but where $\sigma(B)$ and $\sigma(V)$ are from the independent work of Stetson and Harris (requiring *summations* on the right-hand sides of these relations).

TABLE 2
Photometric Transformation Coefficients

	$k_{1,1}$ $e(k_{1,1})$	$k_{1,2}$ $e(k_{1,2})$	$k_{1,3}$ $e(k_{1,3})$	k_2 $e(k_2)$	k_3 $e(k_3)$	k_4 $e(k_4)$	k_5 $e(k_5)$	# CCD frames # star measures
U	1.6027	1.6176	1.6097	0.7059	−0.0985	−0.0011	−0.0884	7
	0.0321	0.0417	0.0425	0.0279	0.0748	0.0609	0.0222	77
B	0.0416	0.0801	0.0514	0.3595	−0.0981	0.0178	−0.0541	8
	0.0271	0.0300	0.0303	0.0220	0.0403	0.0301	0.0174	106
V	0.4298	0.4543	0.4395	0.2278	0.0807	−0.0138	−0.0543	9
	0.0209	0.0227	0.0229	0.0169	0.0307	0.0227	0.0119	121
R	0.4485	0.4724	0.4746	0.2004	0.1735	−0.0601	−0.1126	8
	0.0304	0.0332	0.0334	0.0240	0.0712	0.0517	0.0423	101
I	1.4221	1.4362	1.4281	0.1679	0.0055	0.0013	−0.0299	10
	0.0261	0.0282	0.0286	0.0200	0.0705	0.0504	0.0550	118

$$b-B=k_{1,j}+k_2X+k_3(B-V)+k_4X(B-V)+k_5(B-V)^2, \quad (1b)$$

$$v-V=k_{1,j}+k_2X+k_3(B-V)+k_4X(B-V)+k_5(B-V)^2, \quad (1c)$$

$$r-R=k_{1,j}+k_2X+k_3(V-R)+k_4X(V-R)+k_5(V-R)^2, \quad (1d)$$

$$i-I=k_{1,j}+k_2X+k_3(R-I)+k_4X(R-I)+k_5(R-I)^2, \quad (1e)$$

using the matrix inversion method described by Harris et al. (1981). X is the airmass of the observation, and $j=1,2,3$ represents each night of the observation. Each measured M92 magnitude was assigned a weight, w_m, determined for example in the case of the V band as

$$w_m^2=[\sigma_m^2(v)+\sigma_m^2(V)]^{-1}. \quad (2c)$$

The fits proceeded iteratively, with occasional stars having widely deviant residuals deleted from the fit upon each iteration. Experiments fitting the data with separate airmass terms for each night were not significantly better, and, in any case, were much more poorly constrained for some nights, so we chose to determine a single extinction coefficient for the entire run. To check and account for systematic magnitude errors due to shutter-timing errors, aperture-size errors, and any slight nonphotometric conditions in the M92 data, we determined the mean residual in the stellar magnitude for all standard stars on each frame. In the absence of systematic errors, this residual should approach zero for large numbers of stars. Before the final transformation coefficients k were determined, each frame was offset in magnitude by the weighted[7] mean residual of all stars in the frame to the expected values. For the R and I bands, these offsets were smaller than 0.008 mag; for the B and V bands, these offsets were occasionally as high as 0.02 mag; and several U frames needed offsets of as much as 0.03 mag. For the UBV fits, the process was iterated after the offsets to improve the overall transformation solutions.

Table 2 gives the constants k we obtained for each passband. The zero-points reflect the offset of the CCD measures of $-2.5\log_{10}$ (counts)+24.0, where the aperture counts are normalized to 1 s and are the result of a 10.5 electron ADU^{-1} gain in the CCD electronics. We note that the zero-point constants, $k_{1,i}$, vary from night to night by typically no more than the one-sigma error in their determination (generally less than 1%–2% and by no more than 4%). Moreover, these variations are, with one minor exception in the R band, correlated from band to band in that for each band $k_{1,2}>k_{1,3}>k_{1,1}$. This suggests that they are effectively monitoring nightly differences in atmospheric conditions. The remaining constants k are relatively near those reported by Bushouse (1985) for the same chip and $BVRI$ filters, although the extinction coefficients k_2 we find are generally larger than his (by 0.04–0.06 for $BVRI$, and by 0.15 for U, where, however, we have used the Mould glass U filter rather than the liquid $CuSO_4$ used by Bushouse). Jacoby and Kinman (1986) pointed out some "deterioration" of the Mould filter set and this was noted at about the time of the observations, but this might only account for some of the differences in the k_3 and k_4 constants compared to those reported by Bushouse, and not the k_2 coefficients. Moreover, our B and V extinction coefficients are larger than those found by Stetson and Harris (1988) taken only a few nights later on both the KPNO 0.9- and 4-m telescopes, although we note that their B and V extinction coefficients are smaller than those of Bushouse (1985) by about the same amount as ours are larger than Bushouse's. It is not clear why we found larger extinction coefficients than previous users of the same filter system.

Figure 2 shows the residuals, in the sense of our measures minus the Table 1 values, to the Table 2 fits as a function of stellar color and airmass of the M92 standards. It can be seen that several stars have consistently nonzero residuals, but it is not obvious whether this is a problem with the adopted Table 1 values or our fits. It may also be seen that, despite the observation by other authors (cf. Stetson and Harris 1988) on the need for third-order color terms in some transformation solutions (e.g., in the B band) with this particular filter set, the introduction of such additional detail is not obviously warranted by our own limited data set.

3.3 SA 57 and Hercules Magnitudes

B and V magnitudes for the target SA 57 and Hercules objects were determined iteratively using the constants in

[7]This weighting accounted not only for the random photometric error of each measurement, but also on the number of measurements which entered into the determination of the mean magnitude for each particular standard star.

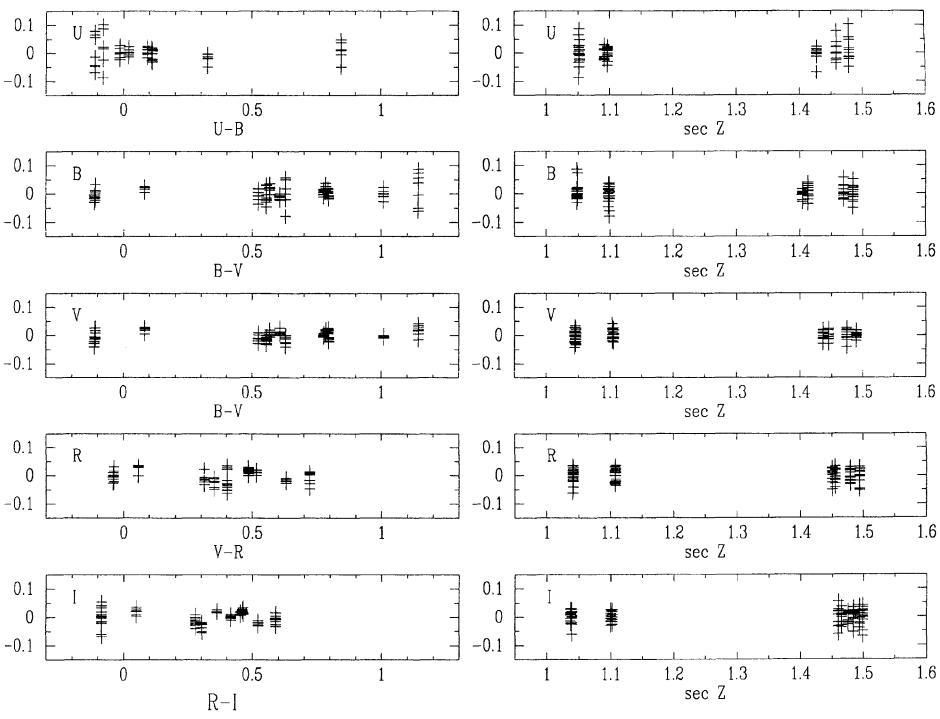

FIG. 2—Residuals to the fits of Eq. (1) and constants in Table 2 to the M92 standard stars in Table 1, as a function of color and airmass. Residuals are in the sense of our magnitudes minus the Table 1 magnitudes.

Table 2 and Eqs. (1b) and (1c). Initially, the choice of sequence objects was made quite liberally, with 55 stars and compact galaxies selected in SA 57 and 36 in Hercules. The final sequences we have elected to present here (in Tables 3 and 4) represent those objects with the smallest random errors (usually those with $e<0.1$ mag) with a reasonable number of measures remaining after the culling of contaminated or bad images. Each image was inspected visually for nearby CCD defects, contamination from neighbors, and cosmic rays by plotting the radial profile about the image centroid. Bad images were eliminated from the solution outright. The occasional remaining, highly deviant photometric measures were eliminated iteratively. The final derived B and V magnitudes were then used to determine the U and R magnitudes using Eqs. (1a) and (1d), respectively, and, finally, the R magnitudes were used to determine the I magnitudes using Eq. (1e). Tables 3 and 4 give the colors and magnitudes for the objects in SA 57 and Hercules, respectively, having the smallest random errors (typically the brightest objects) with a reasonable number of independent measures, in addition to a sampling of stars less well measured but with extreme colors or fainter magnitudes. Errors in the colors represent the quadrature sum of the errors for the respective magnitudes. Figure 3 shows the photometric errors as a function of each magnitude for each of the target stars. Finding charts for these two fields are given in Figs. 4 and 5. Note that charts showing the full photographic survey areas for these two fields are published in Windhorst et al. (1984).

In Tables 3 and 4 we also give coordinates for each object for equinox 1950.0. For the stars in SA 57, accurate relative positions are derived from the astrometry in Majewski (1992) and are for the epoch 1990.0. These have been tied to the AGK-3 via a set of secondary astrometric standards within the plate field and described in Windhorst et al. (1984). The mean circular residual in the global astrometric solution tied to the set of secondary astrometric reference stars across the entire 0.29 deg^2 field was 0.15 arcsec. The Hercules coordinates were derived from FOCAS (Valdes 1982) reductions of full scans of a Mayall 4-m plate of epoch 1985.7 and tied to the secondary standards with a mean circular residual in the global solution across the 0.3 deg^2 field of 0.46 arcsec. The coordinates for the galaxies in SA 57 are taken from a similar reduction as the Hercules data of the Kron (1980) SA 57 catalog and should have a similar accuracy to the Hercules coordinates. Of course the *relative* positions in the smaller CCD fields will be more accurate than the stated global residuals to the absolute positions. We have used all of these coordinate systems in a number of fiber-optic spectroscopy programs using fibers subtending 2 arcsec, and found them to be sufficiently accurate for this purpose.

Several details are worth mentioning concerning the photometric data presented in Tables 3 and 4. We emphasize that the present data were taken primarily for a faint galaxy imaging project, where relatively rough (~5%) magnitude zero-points would have been adequate. The observing procedure was therefore not optimized for calibrating stellar sequences of higher precision than we attempt here. Thus there are a few shortcomings in the calibrations. First, a number of stars in our new sequences are found to have colors outside

TABLE 3
SA 57 Photometric Sequence

nser	α (1950)	δ	$U-B$	$e(U-B)$	$B-V$	$e(B-V)$	$V-R$	$e(V-R)$	$R-I$	$e(R-I)$	Notes
8303	13:06:49.96	29:36:17.9	1.140	0.015[a]	1.039	0.017	0.674	0.018	0.499	0.015	
9801	13:06:45.11	29:38:26.0	1.167	0.053[a]	1.191	0.028	0.752	0.021	0.539	0.020	
10169	13:06:51.15	29:38:59.3	0.836	0.047[b]	1.519	0.044[a]	0.905	0.022[ab]	1.329	0.022[ab]	
9110	13:06:46.66	29:37:27.2	−0.323	0.019	0.512	0.021	0.284	0.032	0.255	0.073	
9928	13:06:49.78	29:38:36.4	0.750	0.045[b]	1.318	0.045[a]	0.883	0.019[ab]	1.084	0.014[ab]	
8408	13:06:55.83	29:36:26.9	−0.179	0.048	0.646	0.041	0.327	0.042	0.144	0.064	
8684	13:06:54.35	29:36:49.8	−0.309	0.046	0.422	0.041	0.335	0.026	0.160	0.090	
8907	13:06:56.63	29:37:09.8	···	···	1.467	0.121[a]	0.933	0.050[ab]	1.330	0.044[ab]	
11201	13:06:50.00	29:40:36.0	···	···	1.328	0.069[a]	0.925	0.061[ab]	1.589	0.060[ab]	
10347	13:06:50.49	29:39:15.5	−0.660	0.099[a]	−0.117	0.104	−0.018	0.066	0.271	0.151	white dwarf
8792	13:06:51.11	29:36:59.0	−0.203	0.053	1.058	0.044	0.532	0.043	0.468	0.043	galaxy
9842	13:06:49.37	29:38:28.1	−0.492	0.037[b]	1.247	0.034[a]	0.712	0.040[b]	0.608	0.029[b]	galaxy
10429	13:06:46.58	29:39:23.1	−0.606	0.063[a]	1.094	0.053	0.510	0.028	0.554	0.029	galaxy
8636	13:06:43.96	29:36:45.8	···	···	1.232	0.040	1.142	0.058[a]	0.768	0.122[ab]	galaxy
9579	13:06:44.89	29:38:08.2	···	···	1.307	0.080[a]	1.223	0.036[ab]	0.757	0.025[ab]	galaxy

nser	U	$e(U)$	$n(U)$	B	$e(B)$	$n(B)$	V	$e(V)$	$n(V)$	R	$e(R)$	$n(R)$	I	$e(I)$	$n(I)$
8303	20.539	0.002	3	19.399	0.015	5	18.360	0.009	7	17.686	0.015	6	17.187	0.001	2
9801	21.274	0.046	7	20.107	0.027	5	18.915	0.009	7	18.163	0.019	6	17.624	0.006	4
10169	22.106	0.020	5	21.270	0.043	5	19.751	0.009	7	18.846	0.020	6	17.517	0.008	4
9110	20.223	0.012	5	20.546	0.014	5	20.034	0.015	7	19.750	0.029	6	19.495	0.067	4
9928	22.167	0.014	4	21.417	0.043	5	20.099	0.012	7	19.216	0.014	6	18.132	0.003	4
8408	20.822	0.035	7	21.001	0.033	3	20.354	0.024	6	20.027	0.034	4	19.883	0.054	3
8684	20.798	0.024	8	21.107	0.039	3	20.685	0.013	3	20.350	0.022	4	20.190	0.087	4
8907	···	···	···	22.413	0.117	5	20.945	0.029	5	20.012	0.041	4	18.682	0.015	3
11201	···	···	···	22.601	0.036	5	21.273	0.059	7	20.348	0.017	3	18.759	0.058	4
10347	21.100	0.023	11	21.760	0.096	4	21.877	0.041	6	21.895	0.051	4	21.624	0.143	4
8792	21.328	0.035	6	21.531	0.040	4	20.473	0.018	7	19.941	0.039	5	19.473	0.019	4
9842	21.587	0.032	10	22.079	0.019	4	20.833	0.028	7	20.121	0.028	6	19.513	0.006	4
10429	21.212	0.043	5	21.818	0.046	5	20.724	0.026	7	20.214	0.010	2	19.660	0.027	4
8636	···	···	···	22.418	0.011	2	21.186	0.038	6	20.044	0.044	2	19.276	0.114	3
9579	···	···	···	22.653	0.076	5	21.346	0.026	5	20.123	0.025	5	19.366	0.004	2

Notes to TABLE 3

[a]This color is out of the range of the M92 calibration star colors used to derive the photometric transformations by more than 0.1 mag. The range of M92 colors used to determine the transformation coefficients is:

$$-0.478<(U-B)<0.844,$$
$$-0.112<(B-V)<1.146,$$
$$-0.041<(V-R)<0.722,$$
$$-0.086<(R-I)<0.589.$$

[b]One of the bands making up this color was determined using another color which was out of range. For example, the B band contributing to the $U-B$ color of star #9928 was derived using a $B-V$ color which was out of range. The R band in the $R-I$ color of star 8636 was derived using a $V-R$ color which was out of range.

the range spanned by the M92 sequence. Technically the Table 2 constants apply only to stars with colors within the span of Table 1 colors. Colors outside this range are obtained through extrapolation of the Table 2 transformations, and are therefore at an increasing risk of systematic errors with larger extrapolations. Note that systematic errors in one band will propagate to adjacent bands in the iterative calculation of colors (objects noted with a "b" in Tables 3 and 4). The objects with colors outside the M92 range are noted with an "a" in Tables 3 and 4.

Second, some SA 57 observations in the R and I bands were made at very high airmass (>1.6) and outside the range used in the determination of the Table 2 constants (see Fig. 2). It was found that for objects with $R-I\gtrsim 0.5$, the high airmass measures in the I band transformed systematically brighter (by an order 0.1 mag) than measures obtained at airmasses in the range used for the calibration. This suggests that higher-order terms than the k_4 term are required in the I band at extremely high airmass. For the $R-I>0.5$ stars, therefore, we have deleted the six high-airmass I-band measurements.

Third, by relying only on the single calibration field of the M92 consortium field, we have determined the constants k with respect to a sequence of stars that are in all likelihood evolved (horizontal-branch stars, subgiants, and giants) globular-cluster stars. In contrast, we expect the majority of our field stars to be on the main sequence. We might then expect some systematic errors in the application of the color

TABLE 4
Hercules Photometric Sequence

nser	α (1950)	δ	U−B	e(U−B)	B−V	e(B−V)	V−R	e(V−R)	R−I	e(R−I)	Notes
6162	17:19:39.81	49:50:43.5	0.493	0.007	0.850	0.008	0.476	0.019	0.431	0.020	c
5695	17:19:46.64	49:49:48.3	0.026	0.010	0.651	0.008	0.380	0.014	0.317	0.013	c
5856	17:19:50.55	49:50:05.6	0.152	0.007	0.722	0.018	0.433	0.018	0.372	0.010	
6169	17:19:34.50	49:50:44.8	−0.229	0.016	0.474	0.012	0.303	0.054	0.284	0.072	
6488	17:19:46.25	49:51:19.1	0.336	0.011	0.814	0.011	0.518	0.013	0.410	0.015	
6336	17:19:44.27	49:51:01.5	0.712	0.013	0.921	0.018	0.570	0.018	0.481	0.017	
6965	17:19:49.78	49:52:13.3	0.347	0.069	0.898	0.028	0.556	0.065	0.561	0.084	d
6986	17:19:40.05	49:52:16.6	···	···	1.788	0.057[a]	0.992	0.054[ab]	1.750	0.011[ab]	
6764	17:19:40.35	49:51:52.2	0.748	0.061[b]	1.327	0.026[a]	0.871	0.028[ab]	0.691	0.031[ab]	e
5677	17:19:43.10	49:49:46.8	1.187	0.052[a]	1.233	0.048	0.713	0.029	0.680	0.019	
6158	17:19:40.88	49:50:43.1	···	···	1.682	0.103[a]	0.923	0.051[ab]	1.562	0.022[ab]	d
7086	17:19:49.93	49:52:30.7	···	···	1.180	0.140	0.960	0.116[a]	1.271	0.038[ab]	
5370	17:19:46.08	49:49:16.0	0.086	0.105	0.890	0.113	0.329	0.073	0.447	0.092	
7313	17:19:49.59	49:52:54.7	−0.209	0.033	1.175	0.039	0.711	0.030	0.658	0.015	galaxy
5786	17:19:35.15	49:50:00.5	0.502	0.051[b]	1.535	0.020[a]	1.040	0.012[ab]	0.775	0.023[ab]	galaxy
5957	17:19:44.00	49:50:18.4	−0.686	0.084[a]	0.979	0.108	0.469	0.095	0.495	0.134	galaxy[e]
7247	17:19:44.46	49:52:48.3	−1.019	0.065[a]	0.309	0.094	0.393	0.078	0.609	0.115	galaxy
6459	17:19:50.12	49:51:14.6	−0.852	0.089[a]	0.530	0.140	0.399	0.137	0.435	0.076	galaxy

nser	U	e(U)	n(U)	B	e(B)	n(B)	V	e(V)	n(V)	R	e(R)	n(R)	I	e(I)	n(I)
6162	18.248	0.006	8	17.755	0.004	6	16.905	0.007	5	16.429	0.018	5	15.998	0.008	7
5695	18.495	0.009	4	18.469	0.004	3	17.818	0.007	5	17.438	0.012	5	17.121	0.005	7
5856	18.927	0.004	7	18.775	0.006	6	18.053	0.017	3	17.620	0.006	4	17.248	0.008	5
6169	18.676	0.011	4	18.905	0.012	2	18.431	0.003	2	18.128	0.054	1	17.844	0.048	1
6488	20.124	0.010	8	19.788	0.005	6	18.974	0.009	5	18.456	0.010	5	18.046	0.012	6
6336	20.728	0.007	3	20.016	0.011	6	19.094	0.014	5	18.524	0.011	5	18.043	0.013	7
6965	21.464	0.067	5	21.117	0.017	4	20.219	0.022	2	19.663	0.062	2	19.102	0.056	3
6986	···	···	···	22.082	0.020	6	20.294	0.053	5	19.302	0.007	5	17.552	0.008	6
6764	22.456	0.059	8	21.708	0.014	5	20.831	0.022	5	19.510	0.018	5	18.819	0.025	6
5677	22.893	0.034	6	21.706	0.039	6	20.473	0.028	5	19.760	0.008	5	19.080	0.017	7
6158	···	···	···	22.383	0.090	6	20.701	0.049	5	19.778	0.013	5	18.216	0.018	6
7086	···	···	···	22.887	0.080	4	21.707	0.114	3	20.747	0.021	4	19.476	0.032	3
5370	22.684	0.040	8	22.598	0.098	6	21.709	0.057	5	21.380	0.045	5	20.933	0.079	6
7313	21.314	0.021	8	21.523	0.026	5	20.348	0.029	5	19.637	0.009	3	18.979	0.012	5
5786	22.433	0.047	4	21.931	0.019	3	20.396	0.007	2	19.356	0.009	4	18.581	0.021	4
5957	21.860	0.049	8	22.546	0.068	6	21.567	0.084	4	21.098	0.044	5	20.603	0.126	7
7247	21.197	0.021	6	22.216	0.061	6	21.907	0.071	5	21.514	0.032	5	20.905	0.111	4
6459	21.698	0.040	6	22.550	0.080	6	22.020	0.115	3	21.621	0.074	5	21.186	0.019	3

Notes to TABLE 4

[a]As in Table 3.
[b]As in Table 3.
[c]Nearby faint star contaminating apertures by less than 1%.
[d]Contamination of apertures by nearby star, possibly by more than 1%.
[e]Contamination of *R* aperture by nearby object.

terms in Eqs. (1) insofar as the detailed spectral energy distributions of main-sequence and evolved stars of similar colors differ. These differences may explain some of the divergence from expected results in the extrapolations to stars of more extreme color that we describe below.

We have processed the data for five bright galaxies in each of the two fields in a manner similar to that described for the stars. These data are also listed in Tables 3 and 4, but we stress *caveat emptor* in the use of the galaxy magnitudes for several reasons. First, while only galaxies with more compact profiles were calibrated, it is expected that smaller fractions of total galaxian light are included within the apertures selected, compared to stellar-light profiles. Second, these aperture sizes used to match the stellar PSFs do not necessarily encircle a constant fraction of galaxy light from frame to frame. This is especially important in consideration of the colors, where some systematic errors may exist from different mean apertures used. In particular, note from Fig. 1 that the mean *stellar* FWHM varies from band to band in any given field, which translates to different fractions of the galaxian-light profiles being measured in each band (though these occur at large radii and therefore near the converging parts of the integrated light profiles because of the 3×FWHM radius apertures). Finally, the spectral-energy distributions of galaxies are not necessarily similar to those of

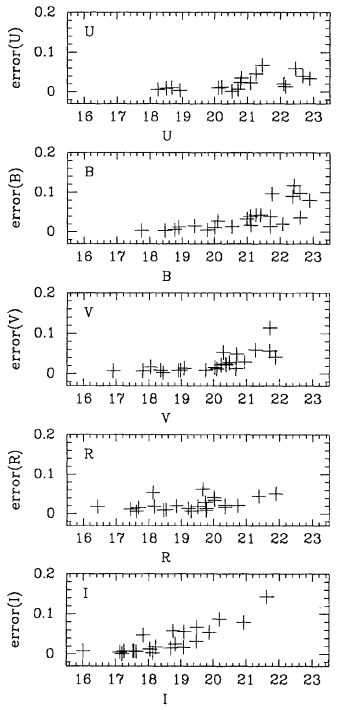

FIG. 3—Random photometric errors as a function of magnitude for the Hercules and SA 57 standard stars. Errors for galaxies are not shown.

individual stars, and so the constants in Table 2 do not strictly apply in the case of galaxies.

4. DISCUSSION

4.1 Color–Color Distributions

In Fig. 6 we show the $(U-B,B-V)$ and $(V-R,R-I)$ diagrams for the stars in Tables 3 and 4. In the left panels, the ridge lines show the Hyades main sequence (lower line) and the limit of metal-poor stars (upper line), as given by Sandage (1969). The region enclosed by the dotted box represents the range of colors encompassed by the M92 calibrators in Table 1. Error bars are shown but in most cases are smaller than the symbol size (galaxies are shown in panels c–f only by error bars). It can be seen that within the dotted box there is a relatively close association of the stellar colors we have found and the expected range of F, G, and K stars. Several stars within the dotted box fall outside the Sandage loci, but not by more than 1–2 sigma.

A few points are worth mentioning with regard to Fig. 6. The six brightest Hercules stars in Table 4 are those enclosed within the Sandage loci, and they progress towards decreasing normalized ultraviolet excess, $\delta_{0.6}$, with increasing $B-V$ color; that is, the change in their proximity to either the metal-rich or metal-poor loci is a function of their color. This effect is a result of the interplay of distance modulus and Galactic metallicity gradients for field stars selected within a limited apparent magnitude range; this behavior can also be seen, for example, in Fig. 6 of Majewski (1992). For stars in a relatively small magnitude range (in this case $17 \leq V \leq 19$), bluer stars are more distant and therefore, on average, more metal poor. A continuation of this trend might also explain the location of the three F–G stars in SA 57, which are not only fainter by more than a magnitude than the six Hercules stars, but in a direction looking straight out of the Galactic plane ($b=89°$) compared to the lower latitude ($b=35°$) Hercules field. Distances of 13–26 kpc from the Galactic plane are estimated for these three stars in Majewski (1992), under the assumption that they are subdwarfs. However, that all three SA 57 F–G stars presented here should lie just above the limit for metal-poor stars is suspicious, and suggests some systematic error. In the photographic analysis of Majewski (1992),[8] the star 9110 was also found to have an extreme ultraviolet excess, but stars 8408 and 8684 were found to have relatively *small* ultraviolet excesses. However, note that the latter two stars are 0.6 mag fainter in U than 9110, and within 0.7 mag of the U limit of 21.5 imposed by Majewski (1992) in his work. We suspect that the CCD data are closer to the truth than the photographic data in the case of the two faint F–G stars, possibly due to a breakdown in the profile-fitting at faint U in the latter. Still, the possibility that some other systematic error remains in the U-band CCD data warrants further investigation.[9]

The very blue star 10347 in SA 57 lies just beyond the Table 1 color-calibration range. On the basis of its colors as well as its very large proper motion at its apparent magnitude (that is, its placement in the reduced proper motion diagram $[B-V,\ H_V=V+5\ \log\ \mu+5]$), we strongly suspect this star to be a white dwarf (see Koo et al. 1986, where the star is identified as No. 65 and also Majewski et al. 1994). While such a blue field star would normally be a valuable commodity in a photometric sequence, we have some concern that star 10347 might be variable. This star was not detected as such in the variability analysis of Trevese et al. (1994), but a separate analysis of this star (with additional plate material) by Majewski et al. (1992) does show some hint of variability at the level of 0.10–0.20 mag (about 1-σ) during the years 1987–1990.

Six stars in the two fields lie redward of the dotted box in the $(U-B,B-V)$ diagrams, and show a large scatter from an extrapolation of the FGK star loci, despite rather small random error bars. We regard as unlikely that these stars might represent some population which might have intrinsically different colors than those represented by the loci. For example, the suspect stars do not show any peculiar deviation from the main color loci of stars in our *photographic*

[8]It might be argued that since the photographic survey of Majewski (1992) made partial use of preliminary reductions of the present data, that they are not wholly independent. But note that the *relative* magnitudes and colors in Majewski (1992) are photographically derived and the CCD data only participated in setting the absolute colors and magnitudes. Thus, for example, star 9110 was found to have an extreme ultraviolet excess compared to other stars within the photographic survey.

[9]It is possible that these stars lie outside the Sandage loci because they are binaries, but it is unlikely that we would encounter three such cases so closely placed in the sky. They might also not be subdwarfs, but again, we consider that we would encounter three evolved stars unlikely, especially given the greater photometric parallaxes implied in that case. Finally, it is possible that the Sandage locus for the metal-poor limit is too low. Consideration of this prospect is beyond the scope of this paper.

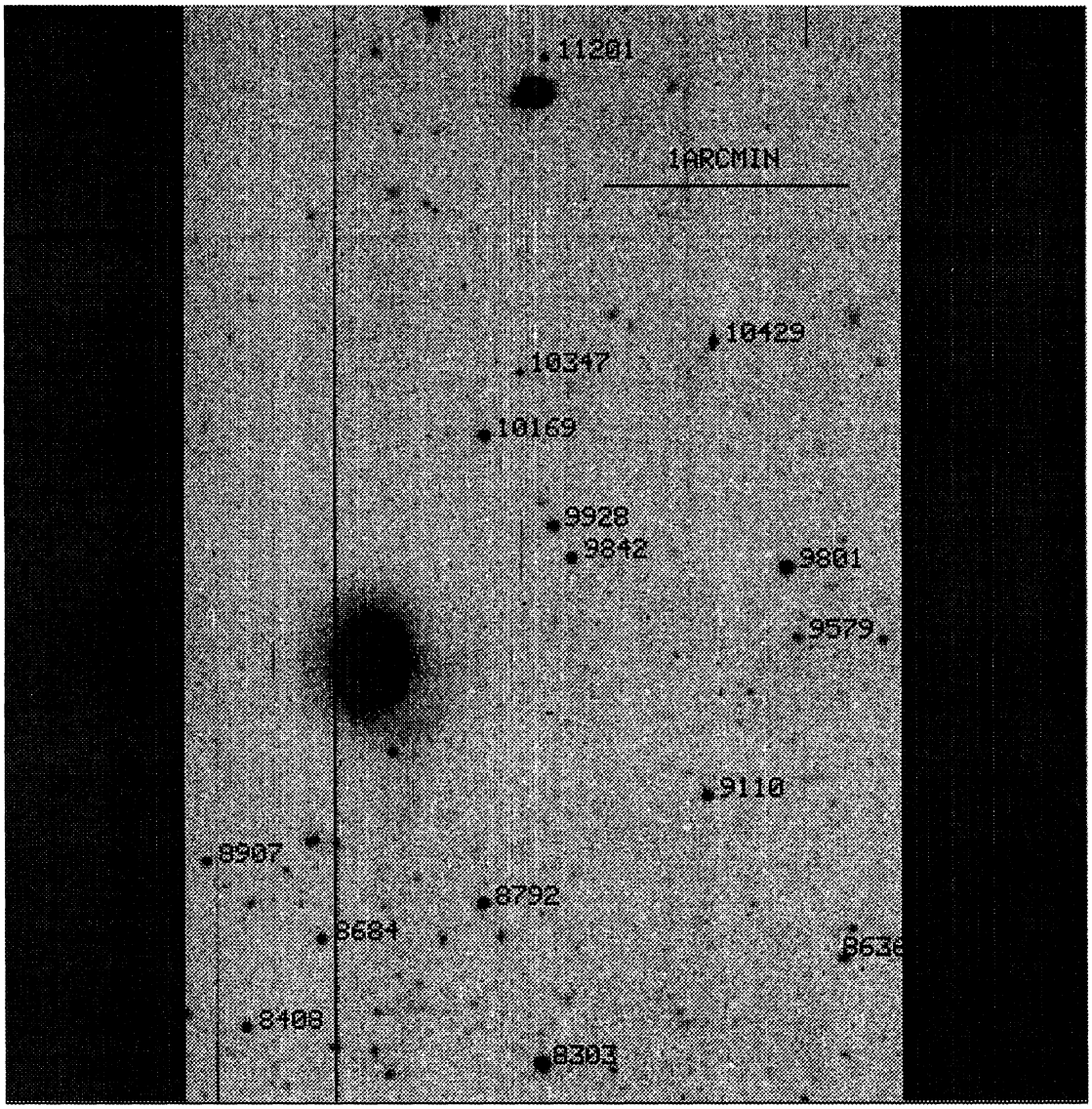

FIG. 4—Finding chart for the SA 57 field from a typical V exposure with the RCA #1 camera. Objects lie to the lower left of the first digit of their identifications. North is up and east is to the left. Several bad columns on the chip may be seen.

photometry. This scatter probably represents a rather quick deviance of our extrapolations of Eqs. (1) past the color range of the M92 stars, and we caution against trusting the $(U-B)$ and $(B-V)$ colors in Tables 3 and 4 for stars with $B-V>1.3$.

The right-hand panels in Fig. 6 show the distribution of our CCD data in the $(V-R,R-I)$ diagram. The upper line in panels (b), (d), and (f) is the locus for stars found in the Gliese catalog by Bessel (1990), while the lower solid line is the second locus seen in Landolt (1992). Again, it can be seen that stars within the dotted box show much better agreement with the loci than those stars outside the M92 calibration range. The points most deviant from the solid lines and within the dotted box are also those with the largest error bars. There is clearly a systematic deviation in the colors of the latest spectral types in both the SA 57 and Hercules fields from the Bessell and Landolt loci. Originally, we were inclined to attribute this deviation to systematic errors in the CCD photometry for stars with $R-I\gtrsim 1.0$, which is outside the color range of the M92 calibration stars. However, in their *VRI* photometric study of faint stars, Richer and Fahlman (personal communication) have identified a similar deviation in the $(V-R,R-I)$ diagram; it is possible that these faint M dwarfs represent a distinctly different population (a more metal-poor, Population II?) than the solar neighborhood.

In summary, we find reasonably good agreement in the color distributions for those stars within the color range spanned by the M92 stars in Table 1, but evidence of possible systematic errors for those stars outside this range.

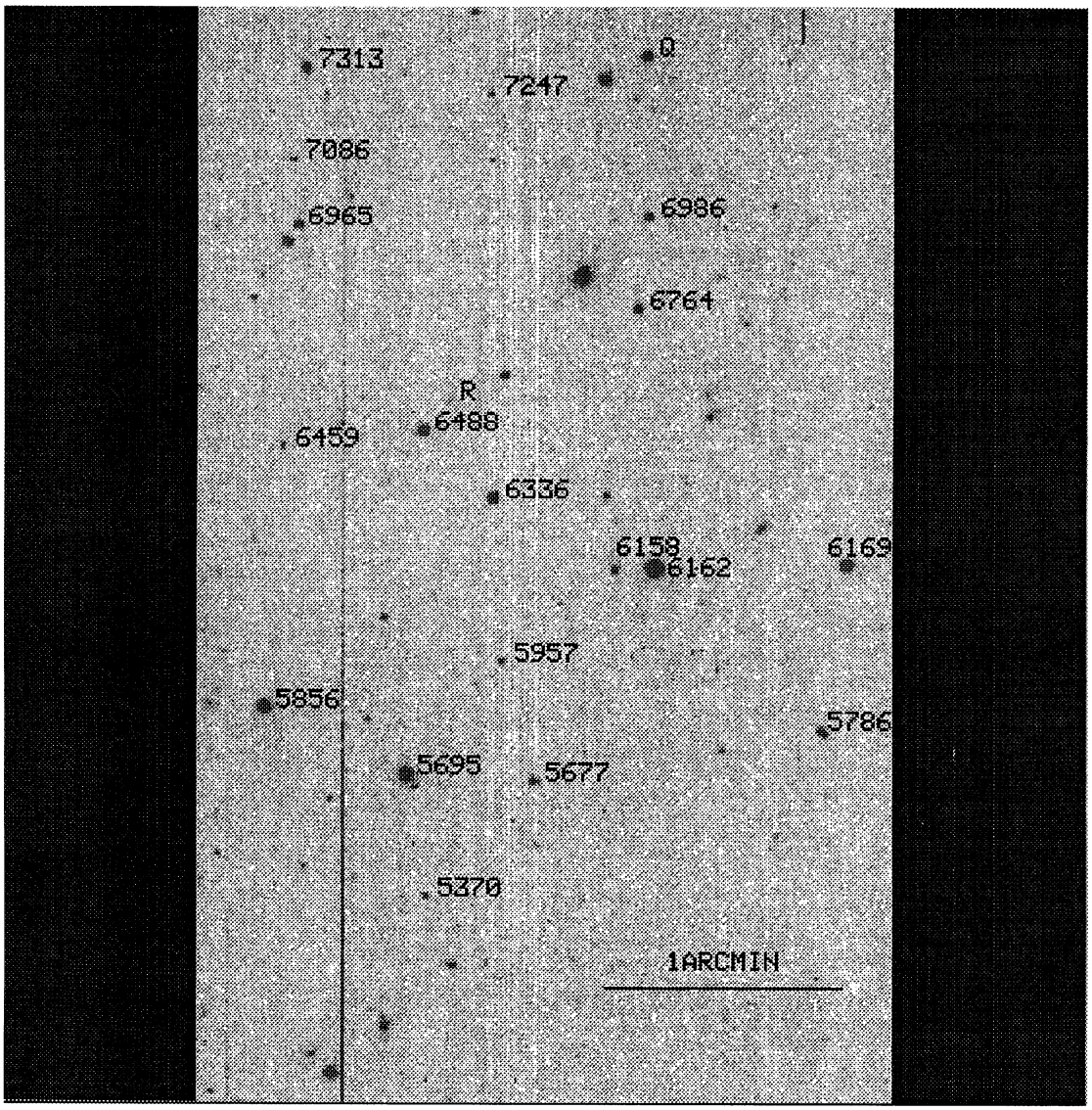

FIG. 5—Finding chart for the Hercules field from a typical V exposure with the RCA#1 camera. Object marked "Q" is a $z=1.04$ QSO, while the object marked "R" is the radio galaxy 53W077 (see Windhorst et al. 1984). Objects lie to the lower left of the first digit of their identifications. North is up and east is to the left.

While it limits the number of useful stars for calibration purposes, we think it prudent to make use of only the stars without footnotes a or b in Tables 3 and 4. This still leaves a suitable number for setting magnitude and color zero-points in deep catalogs of stars, galaxies, and QSOs, and in the next section we make use of these stars to recalibrate our own catalogs. Given the various limitations of the present data, we encourage additional work to expand the usefulness of these calibration sequences.

4.2 Magnitude Corrections to Photographic Catalogs

We now discuss the accuracy of the magnitude zero-points in the catalogs from which we have been working on surveys of stars, galaxies and QSOs. Details on the derivation of the prevailing photographic J and F magnitude zero-points in the SA 57 field are described in Kron (1980) and for the U and N bands in Koo (1986). It is sufficient to say here that while sequences of B and V magnitudes that exist in these fields have made us reasonably confident in the J and F magnitude zero-points, the setting of the U and N zero-points has been less direct due to a meager number of faint stellar calibrators in the former and a total lack of I-band standards for the latter. Koo (1986) gives the expected error in the setting of the U and N zero-points in our SA 57 catalog as $\pm 0.05-0.06$ mag. Further discussion of existing photometric sequences in the SA 57 field is given in

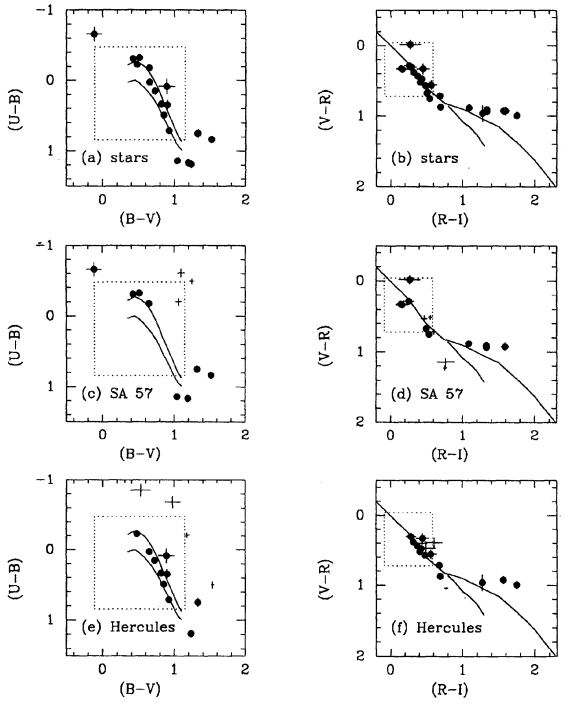

FIG. 6—Color–color distributions for the objects in Tables 3 and 4. Solid circles show stars; in most cases, the one-sigma random error bars are smaller than the symbol. Error bars without circles are for the galaxies. Panels (a) and (b) show the distributions for all SA 57 and Hercules stars in Tables 3 and 4. Panels (c) and (d) show the distributions for only the SA 57 objects, but for both stars and galaxies. Panels (e) and (f) show all Hercules objects. In the left-hand panels (a), (c), and (e), the lower solid lines show the locus of stars in the Hyades and the limit for the most extremely metal-poor stars, as calculated by Sandage (1969). In the right-hand panels (b), (d), and (f), the upper solid line is the locus for stars found in the Gliese catalog by Bessel (1990), while the lower solid line is the second locus seen in Landolt (1992). In all panels, the dotted lines show the area spanned by the color distribution of the stars in the calibration field, M92.

Majewski (1992) and Bershady et al. (1994; see also the discussion in the Appendix), where use is made of other calibration material in addition to preliminary reductions of the present data.

TABLE 5
Photographic Catalog Magnitudes for SA 57 Objects

nser	*U*	*J*	*F*	*N*
8303	20.173	19.310	18.120	17.034
9801	20.953	19.849	18.508	17.575
10169	22.277	20.785	19.159	17.501
9110	20.165	20.400	19.896	19.391
9928	22.519	21.157	19.542	18.135
8408	20.805	20.845	20.158	19.458
8684	20.616	20.944	20.503	20.039
8907	24.470	21.983	20.330	18.715
11201	···	22.514	20.734	18.725
10347	21.018	21.761	21.701	21.654
8792	21.513	21.179	20.233	19.397
9842	21.467	21.646	20.384	19.349
10429	21.381	21.445	20.405	19.950
8636	23.155	22.294	20.280	19.152
9579	24.459	22.411	20.591	19.321

TABLE 6
Photographic Catalog Magnitudes for Hercules Objects

nser	*U*	*J*	*F*	*N*
6162	18.41	18.50	17.08	16.70
5695	18.73	18.93	17.78	17.33
5856	19.04	19.10	17.91	17.44
6169	18.83	19.17	18.25	17.85
6488	20.03	19.81	18.71	18.06
6336	20.56	19.98	18.77	18.02
6965	21.34	21.02	19.98	19.18
6986	22.51	21.39	19.64	17.64
6764	22.43	21.31	19.81	18.63
5677	22.19	21.40	20.00	19.01
6158	23.19	22.02	20.11	18.20
7086	23.63	22.80	21.11	19.35
5370	22.47	22.27	21.41	21.04
7313	21.27	21.27	19.93	18.99
5786	22.40	21.55	19.70	18.54
5957	21.64	22.05	21.23	21.05
7247	21.39	22.63	21.88	20.32
6459	21.57	22.30	21.81	20.75

Our Hercules catalog is relatively new, and is first described in the QSO survey described in Kron et al. (1992). This field presently has no published photoelectric sequences and the *UJFN*-magnitude zero-points of our corresponding catalog have been set using a preliminary reduction of the data described here.

In Table 5 for SA 57 and Table 6 for Hercules we give our catalog *UJFN* magnitudes for the CCD sequence objects. In Fig. 7 for SA 57 and Fig. 8 for Hercules we compare these *UJFN* magnitudes to the *UJFN* magnitudes derived by transforming the *UBVRI* magnitudes from this paper into the

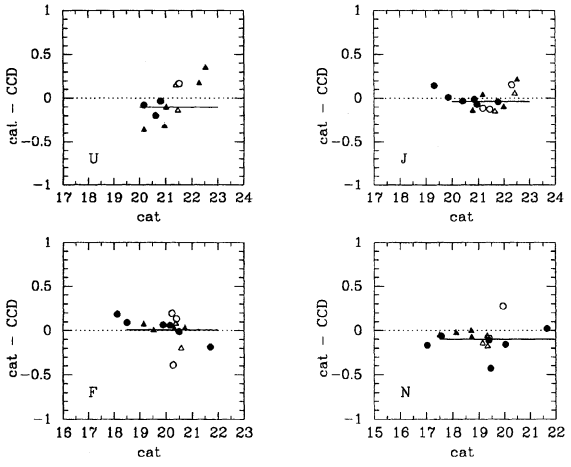

FIG. 7—The difference between *UJFN* photographic magnitudes in our catalogs and the *UJFN* magnitudes obtained by transforming the SA 57 *UBVRI* magnitudes in Table 3 via the equations in Table 5 of Majewski (1992). The abscissa shows the catalog *UJFN* magnitudes. Solid symbols show stars and open symbols show galaxies. In each case, *triangles* show less reliable objects having footnotes a or b in Table 5, and *circles* show the more reliable objects not requiring extrapolation of Eqs. (1). The *solid lines* in each panel represent the best weighted fit (given in Table 5) to those *solid circles* in the unsaturated regimes of the photographic plates. Note that only the *solid circles* are used in the calibrations in Table 5.

TABLE 7
Calibration of *UJFN* Photographic Catalogues

	SA 57	Hercules		
$U_{cat}-U_{CCD}$		$-0.174\,U_{cat}+3.408$	(5 pts, rms=0.041)	$U_{cat}<20.45$
	-0.104 (3 pts, rms=0.071)	-0.150	(4 pts, rms=0.047)	$U_{cat}>20.45$
$J_{cat}-J_{CCD}$		$-0.523\,J_{cat}+10.544$	(6 pts, rms=0.080)	$J_{cat}<20.05$
	-0.036 (4 pts, rms=0.021)	$+0.060$	(4 pts, rms=0.122)	$J_{cat}>20.05$
$F_{cat}-F_{CCD}$		$-0.435\,F_{cat}+7.922$	(3 pts, rms=0.008)	$F_{cat}<18.15$
	0.008 (4 pts, rms=0.105)	$+0.026$	(7 pts, rms=0.059)	$F_{cat}>18.15$
$N_{cat}-N_{CCD}$		$-0.727\,N_{cat}+12.818$	(3 pts, rms=0.026)	$N_{cat}<17.66$
	-0.100 (5 pts, rms=0.160)	-0.020	(6 pts, rms=0.065)	$N_{cat}>17.66$

UJFN system via the transformation equations given in Table 5 of Majewski (1992). We discuss the nature of this comparison for Hercules first (Fig. 8). The CCD data are compared to the photographic magnitudes measured within a 2 arcsec radius aperture in our catalogs as generated by the FOCAS software. For the reasons we have outlined in previous sections, we will ignore the galaxies and focus our attention on only those stars without footnotes a or b in Tables 3 and 4 (these are shown as *solid circles* in Fig. 8). The most obvious feature in each panel of Fig. 8 is the increasing magnitude error in the plate magnitudes with increasing brightness as a result of the onset of image saturation in the photographic plates. The onset of saturation for stars occurs more or less gradually depending on the bandpass. However, because the number of points is small, we fit each photographic correction with a simple linear function for the saturated region and an offset in the unsaturated region. We bother to deal with the saturated regime at all because we hope to make some use of the brighter star data in future papers regarding the star counts in these fields. The fitted functions are listed in Table 7. The relative weighting for each star is taken as the reciprocal of the error in the magnitude. For the F and N bands the onset of the linear regime is readily identifiable near $F\sim18$ and $N\sim17.5$, and leaves 7 and 6 useful stars, respectively, for setting the faint catalog zero-point. The U and J saturations appear to be more gradual and the choice of the break point in the fit function is more difficult. From previous experience, we believe that sky-limited J plates should be linear by at least $J\sim20.5$; this may be seen for example in Fig. 9 of Kron (1980) where it is shown that the light distribution function (characterized by the r_1 statistic) for unresolved sources on one of our sky-limited J plates is stable by this magnitude. Therefore, we have elected to use only the last four J points to set the J faint-end zero-point. The U data present somewhat of a dilemma. It is not clear whether the point near $U\sim20$ (star 6488) is in the saturated or unsaturated regime. The one magnitude gap near $U\sim19.5$ makes it difficult to discern the nature of the transition. We have elected to use star 6488 in the fits to both regimes.[10] Table 7 shows that, apart from the U band, the zero-point corrections to the catalogs are minor, as expected given that the zero-points were originally set with early reductions of these same CCD data, albeit without as careful a culling of possibly problematical stars.

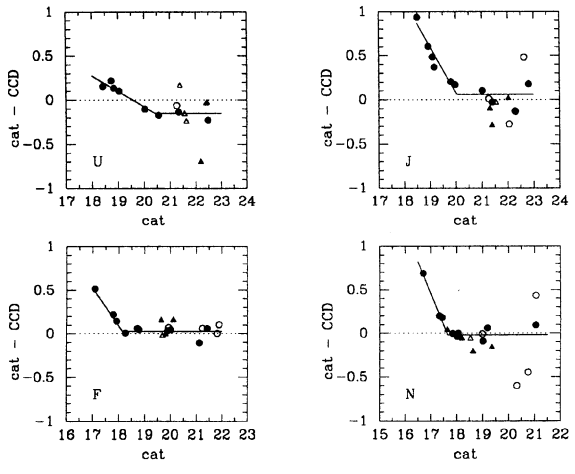

FIG. 8—Same as Fig. 7, except for Hercules objects in Table 4. The rising points at brighter magnitudes reflect the saturation of the photographic plates. *Solid lines* show the two-piece linear fits to the saturated and unsaturated regimes of the photographic magnitudes, as given in Table 5.

There are few bright SA 57 calibration stars, so that we are unable to calibrate the saturation regime for each band. However, a number of brighter SA 57 calibrations exist from other sources (see references in Majewski 1992). In Table 5 we list the zero-point corrections and their errors that we obtain in the unsaturated regime of our SA 57 catalog. Based approximately on the saturated/unsaturated break points in the Hercules catalog, we use only the faintest n stars in each band (as given in Table 7) to determine the faint-end magnitude corrections to the SA 57 catalog. As expected, the J and F corrections we find are negligible, but it is satisfying that the U and N corrections also appear to be within the rms errors of the measurements, given the less direct means by which the zero-points had previously been set.

S.R.M. and M.A.B. were funded by NASA through Grant Nos. HF-1036.01-92A and HF-1028.01-92A, respectively, from the Space Telescope Science Institute, which is operated by the Association of Universities for Research in Astronomy, Incorporated, under Contract No. NAS5-26555, and, while at Yerkes Observatory, by NSF Grant No. AST-8814251. D.C.K. was supported by an STScI Fellowship during the original observations and acknowledges support from NSF PYI AST88-58203.

[10]This was partly out of necessity for the bright end fit, since the four points with $U<19$ alone do not give a sensible saturation fit.

TABLE 8
Comparison of *UJFN* Zero-Points with that Employed in Bershady et al. (1994)

Band	$m-m$ (Bershady et al.)	
	SA 57	Hercules
U	−0.069	−0.010
J	+0.022	+0.140
F	+0.051	+0.221
N	−0.075	+0.100

APPENDIX. COMMENTS REGARDING THE CALIBRATION IN BERSHADY ET AL. (1994)

In another paper (Bershady et al. 1994), where we explore the optical and near-infrared colors of faint galaxies, we have made use of preliminary reductions of the data presented here in order to set the photometric zero-points in the SA 57 and Hercules fields. The zero-points in Bershady et al. were set before several minor adjustments to the CCD calibrations. In addition, that calibration included the reddest stars that in the present paper we have decided not to use, until we understand whether the systematic differences in the expected colors (discussed in Sec. 4.1) represent an intrinsic property of the faint M dwarf population or are the result of systematic photometric error. At the same time, Bershady et al. included additional faint photoelectric sequences from other sources (as did Majewski 1992) as well as slightly different transformation equations from the *UBVRI* to the *UJFN* systems, whereas the calibration of the photographic catalogs discussed here makes use only of the CCD data in this work. Either calibration is a substantial improvement over previous work, as evidenced, for example, by the fact that the stellar loci in the color–color diagrams between our different fields are brought into much better agreement with one another.

In Table 8, we summarize the differences in *UJFN* zero-points obtained if the photometry in Bershady et al. (1994) had instead relied solely on the zero-point offsets presented in Table 7 (excluding the stars falling in the saturated regime). Note that the differences in color zero-points are at most 6% between the systems.

REFERENCES

Bershady, M. A., Hereld, M., Kron, R. G., Koo, D. C., Munn, J. A., and Majewski, S. R. 1994, AJ (in press)
Bessel, M. S. 1990, A&AS, 83, 357
Bohlin, R. C., Turnshek, D. A., Williamson II, R. L., Lupie, O. L., Koorneef, J., and Morgan, D. H. 1990, AJ, 99, 1243
Bushouse, H. 1985, NOAO Newsletter, 4, 14
Chiu, L.-T. G. 1980, ApJS, 44, 31
Christian, C. A., Adams, M., Barnes, J. V., Butcher, H., Hayes, D. S., Mould, J. R, and Siegel, M. 1985, PASP, 97, 363
Hamilton, D. 1985, ApJ, 297, 371
Harris, W. E., Fitzgerald, M. P., and Reed, B. C. 1981, PASP, 93, 507
Heasley, J. M., and Christian, C. A. 1986, ApJ, 307, 738
Jacoby, G., and Kinman, T. 1986, NOAO Newsletter, 7, 15
Koo, D. C. 1985, AJ, 90, 418
Koo, D. C. 1986, ApJ, 311, 651
Koo, D. C., and Kron, R. G. 1988, ApJ, 325, 92
Koo, D. C., Kron, R. G., and Cudworth, K. M. 1986, PASP, 98, 285
Koo, D. C., Bershady, M. A., Wirth, G. D., Stanford, S. A., and Majewski, S. R. 1994, ApJ, 427, L9
Kron, R. G. 1980, ApJS, 43, 305
Kron, R. G., Bershady, M. A., Kron, R. G., Munn, J. A., Koo, D. C., and Majewski, S. R. 1992, in The Space Distribution of Quasars, ASP Conf. Ser. 21, edited by D. Crampton (San Francisco, ASP), p. 32
Landolt, A. U. 1992, AJ, 104, 340
Majewski, S. R. 1992, ApJS, 78, 87
Majewski, S. R., Munn, J. A., Kron, R. G., Bershady, M. A., Smetanka, J. J., and Koo, D. C. 1992, in The Space Distribution of Quasars, ASP Conf. Ser. 21, edited by D. Crampton (San Francisco, ASP), p. 55
Majewski, S. R., Munn, J. A., Kron, R. G., Bershady, M. A., Smetanka, J. J., and Koo, D. C. 1994, in preparation
Sandage, A. R. 1969, ApJ, 158, 1115
Shane, C. D., and Wirtanen, C. A. 1967, Lick Obs. Publ., 22, Part I
Smetanka, J. J. 1994, MNRAS (submitted)
Stetson, P. B., and Harris, W. E. 1988, AJ, 96, 909
Trevese, D., Kron, R. G., Majewski, S. R., Bershady, M. A., and Koo, D. C. 1994, ApJ (in press)
Valdes, F. 1982, FOCAS User's Manual (Tucson, Kitt Peak National Observatory Computer Support Group)
Windhorst, R. A., Kron, R. G., and Koo, D. C. 1984, A&AS, 58, 39